MANIFESTATION OF PEAR-SHAPED CLUSTERS IN COLLINEAR CLUSTER TRI-PARTITION (CCT)

Yu.V. Pyatkov[1,2], D.V. Kamanin[2], A.A. Alexandrov[2], I.A. Alexandrova[2], Z.I. Goryainova[2], V. Malaza[3], E.A. Kuznetsova[2], A.O. Strekalovsky[2], O.V. Strekalovsky[2], V.E. Zhuchko[2]

[1]National Nuclear Research University MEPhI (Moscow Engineering Physics Institute), Moscow, Russia
[2]Joint Institute for Nuclear Research, Dubna, Russia
[3]University of Stellenbosch, Faculty of Military Science, Military Academy, Saldanha 7395, South Africa

INTRODUCTION

The majority of our experiments of recent years were dedicated to the study of new multibody at least ternary decay channel of low excited heavy nuclei [1, 2]. Due to specific features of the effect, it was called collinear cluster tri-partition (CCT). Now we have an entire collection of different CCT manifestations observed through the linear structures in the mass correlation distributions M_1–M_2 of decay products. Some of the structures look like strait lines M_1 = const or M_2 = const. The most populated structures of such sort are aggregated in so called "Ni-bump" which was analyzed in details in our previous publications [3, 4]. More specific structures satisfying the condition $M_1 + M_2$ = const, while the total mass of the fragments involved is less than the mass of the fissioning nucleus were revealed in our recent experiment at the COMETA spectrometer (JINR). The analysis of these structures is presented below.

EXPERIMENTS AND RESULTS

Our latest experiments were dedicated to searching for rare decay modes of low excited actinide nuclei with a special attention the reliability of identification of such events. The improvement of our experimental methods has been achieved by digitizing of a signal from each detector and off-line processing of the signal images. Here we present the results of the experiment (Ex1) performed using such approach. The scheme of the setup is shown in Figure 1. We used the double-armed time-of-flight spectrometer of fission fragments (FFs). Two "start" micro-channel plates based timing detectors *St1* and *St2* were placed in the center of the experimental vacuum chamber. The ^{252}Cf (sf) source was located between the detectors. Four mosaics of eight PIN diodes each provided measuring of both the FF energy and time-of-flight.

The data acquisition system consisted of the fast flash-ADC (Amplitude to Digital Convertor) CAEN DT574 multichannel digitizer, logic blocks providing trigger signals, and a personal computer. Current value of the signal was measured by the digitizer every 0.2 ns.

Time reference point on the PIN diode signal was calculated using a new algorithm proposed by us earlier [5]. The algorithm approximates the initial part of a leading edge of the signal by a parabolic curve under condition that the parabola vertex lies on the mean value of the base line. The second condition to be met consists in sewing of the parabolic curve with a line approximating the linear part of the leading edge. This means that both the values and derivatives of the parabolic and linear functions must be equal in the sewing point. The

parameters of the curve are estimated by a minimization of a χ^2 using some points of the leading edge located above the three sigma (standard deviation of the base line values) level. Experimental testing proved this method to give unbiased "true" time reference corresponding to the real beginning of the signal [5]. Thus, distortion of the time-of-flight due to so called "plasma delay" (PD) [6] is excluded.

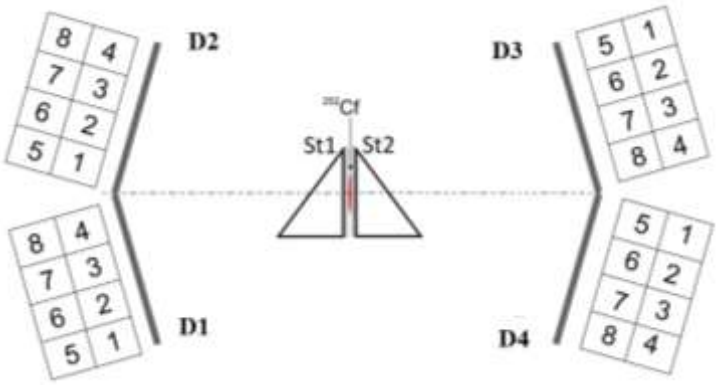

FIGURE 1. Ex1: layout of the experimental setup. The ^{252}Cf (sf) source is placed between two "start" micro-channel plates based timing detectors *St1* and *St2*. Four mosaics (D1÷D4) of eight PIN diodes each provide measuring of both the FF energy and time-of-flight.

Calculation of the FF mass taking into account pulse-height-defect (PHD) based on the parametrization proposed in [7] was performed in the iterative procedure described in [8].

FFs mass correlation distribution in the region of the "Ni-bump" [3] is presented in Figure 2(a). Due to the background conditions of this experiment, the events with the energy of the light fragment in the range E_2 = (6÷30) MeV were selected.

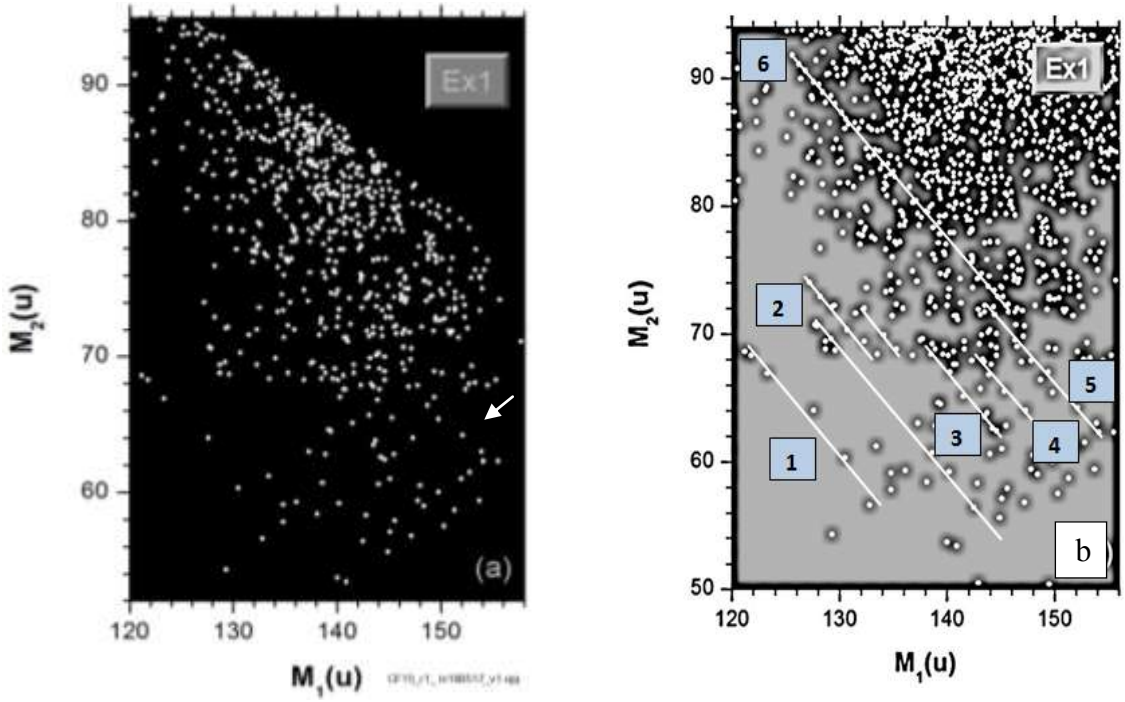

FIGURE 2. FFs mass correlation distributions from ^{252}Cf(sf) obtained in Ex1 – (a). Specific rhombic-spiral structure in the bottom of the figure ("nuclear rose") is marked by an arrow. The same distribution is shown in different graphic presentation in (b). The tilted lines marked by the numbers 1–6 meet the condition $M_1 + M_2$ = const.

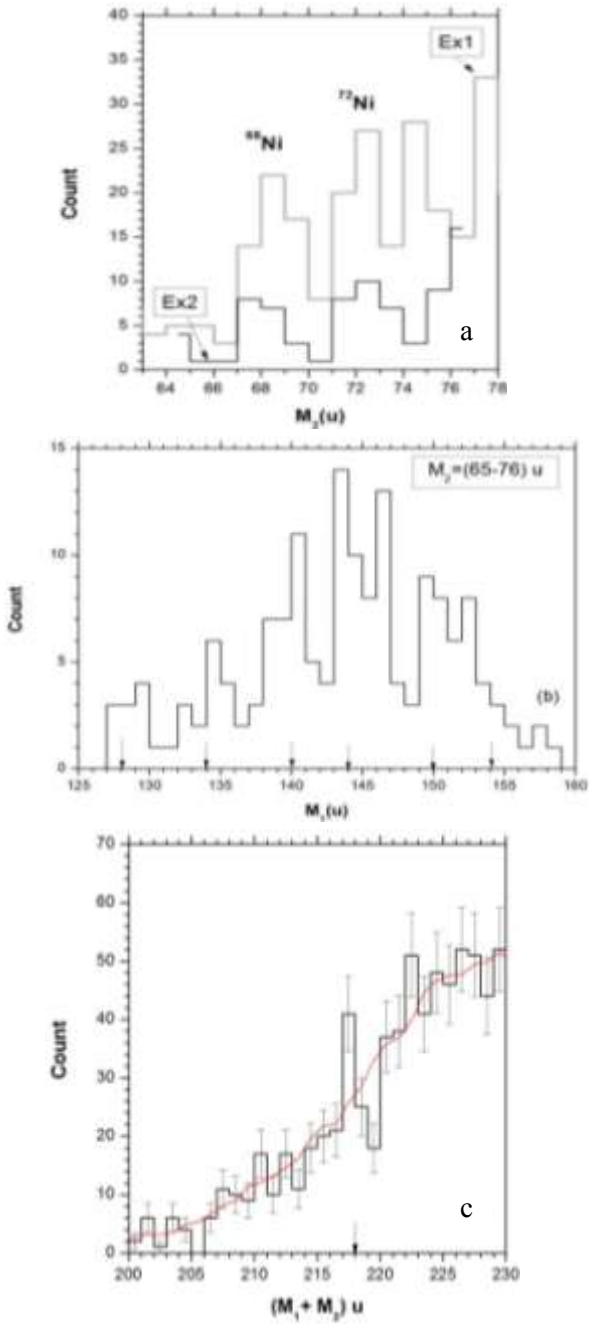

FIGURE 3. Different projections of the mass correlation distribution from Ex1 (Figure 2). Projection of the distribution is compared with that obtained earlier in Ex2 [1] – (a). Projection of the distribution onto M_1 axis under condition that M_2 = (65–76) u – (b). Positions of the magic nuclei are marked by the arrows. Projection of the distribution along the direction $M_1 + M_2$ = const – (c). The peak centered at the mass 218u is marked by the arrow. See text for details.

Different projections of the mass correlation distribution from Ex1 are shown in Figure 3.

As can be inferred from the Figure 2a the statistics in Ex1 is approximately three times more than that in Ex2 [1]. A total yield of two Ni peaks in Ex1 does not exceed 10^{-4} per binary fission which agrees with our previously obtained value. The data of Ex2 indicated that the heavy clusters in the ternary prescission configurations are predominantly magic nuclei (Table 1 in [3]). Noticeably large statistics in Ex1 allowed us to confirm previous observation. The projection of the distribution shown in Figure 2(b) onto M_1 axis for the range of M_2 = (65–76) u clearly demonstrates increased yield of the heavy fragments corresponding to the magic isotopes of ^{128}Sn, ^{134}Te, ^{140}Xe, ^{144}Ba, ^{150}Ce, ^{154}Nd (their masses are marked in Figure 3(b) by the arrows).

The data from Ex1 along with the presence of the lines at the mass numbers A = 128, 68, 72 (Figure 2(a)) similar to those observed in Ex2 show some additional structures. A rhombic-spiral structure in the lower right corner of Figure 2(a) that resembles a rose depiction was called “nuclear rose”. It consists of the family of lines $M_1 + M_2 \approx$ const and several lines almost perpendicular to them. The lines of the first sort (marked by the numbers 1–6 in Figure 2(b)) will be analyzed in the next section while a discussion of the latter is below the scope of this paper.

The longest line 6 in Figure 2b manifests itself not so obviously as the others. Nevertheless, projection of the mass correlation distribution along the direction $M_1 + M_2$ = const demonstrates a statistically significant peak corresponding to this line (Figure 3c). The smoothed background in the figure is shown by the smooth curve.

Figure 4 demonstrates the linear structures from Figure 2b in detail. Presumable prescission cluster composition of the fissioning system for some point lying on the analyzed line is shown in the panels. Corresponding missed cluster in each case is shown first. Nuclear composition of the heavy magic core is marked below the line underlying the chemical symbols of two detected fragments.

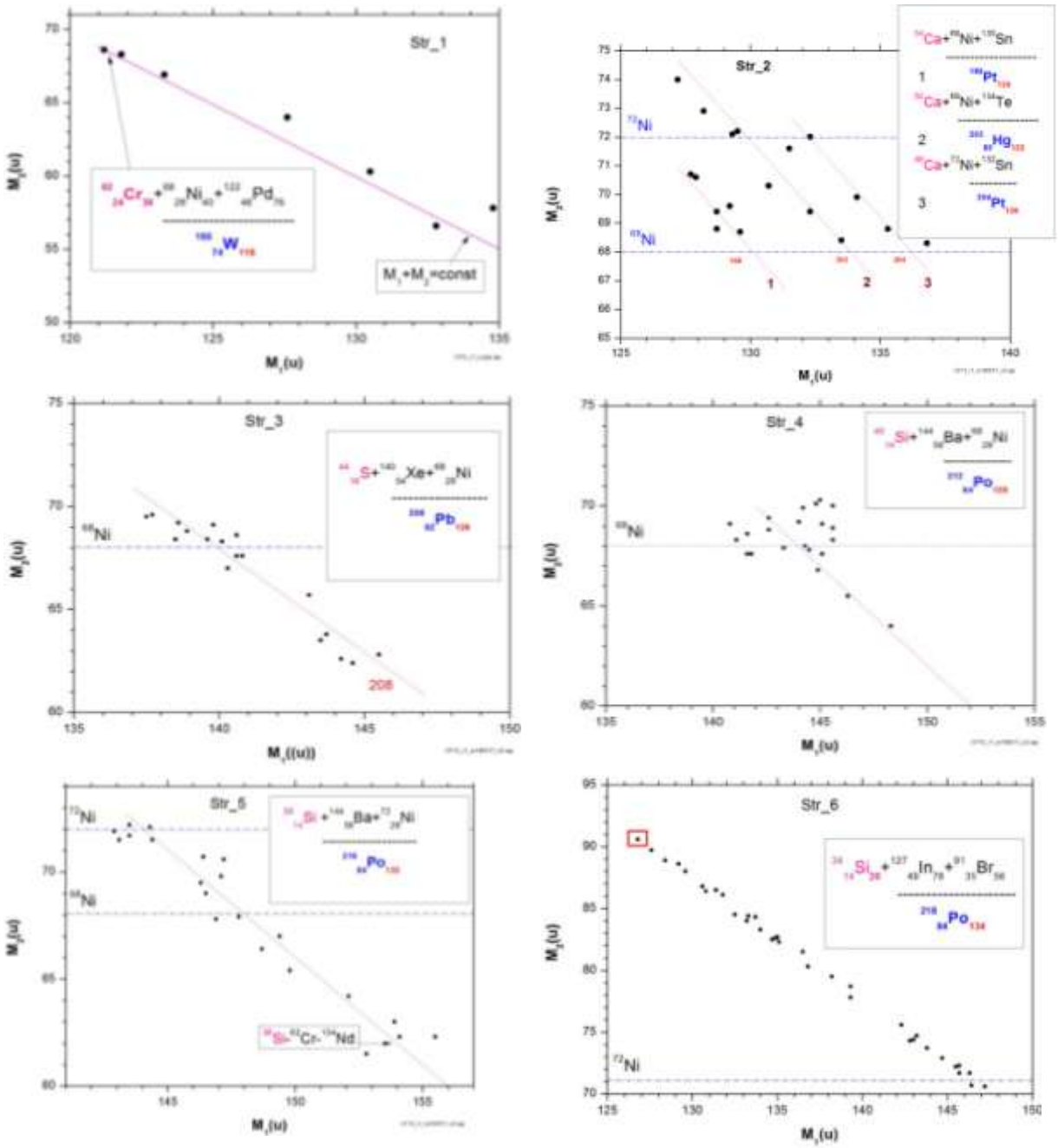

FIGURE 4. Linear structures from Figure 2b shown in detail. Presumable prescission cluster configurations of the decaying system for some points are presented in the panels. Corresponding missed cluster in each case is shown first.

Table 1. Parameters of the linear structures shown in Figure 2b.

Parameters of the structures observed				
Str №	Missing fragment	Heavy magic core	Number of neutrons	Experiments
1	^{62}Cr	^{190}W	116	Ex1
2	$^{48, 50, 54}$Ca	^{198}Pt, ^{202}Hg, ^{204}Pt	120, 122, 124	Ex1 & Ex2
3	^{44}S	^{208}Pb	126	Ex1 & Ex3
4	^{40}Si	^{212}Po	128	
5	^{36}S	^{216}Po	132	
6	^{34}Si (N = 20)	^{218}Po	134	Ex1

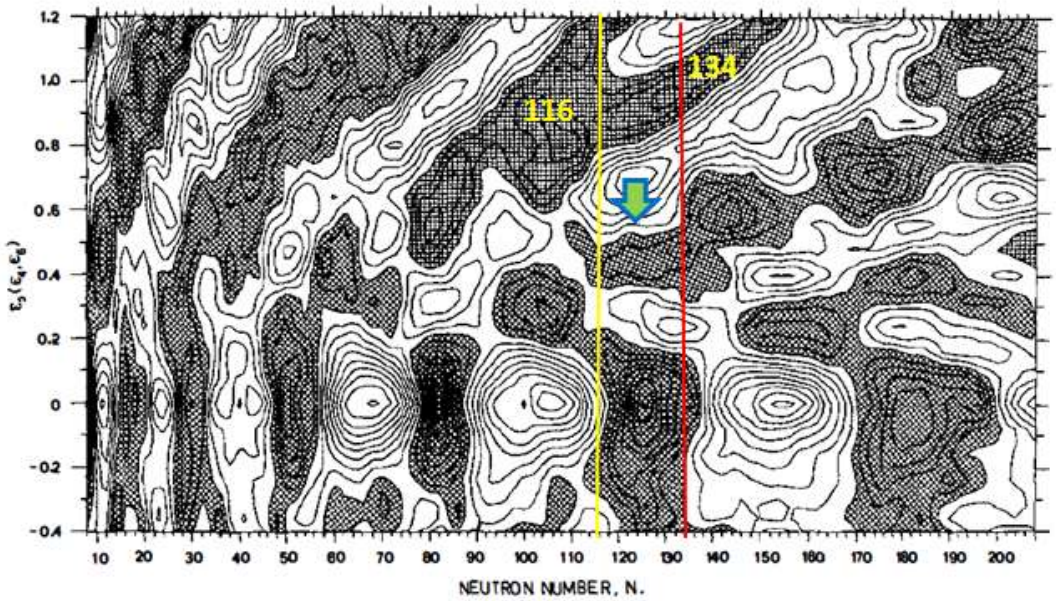

FIGURE 5. Shell energy diagram [10] depending on neutron number and deformation. Areas corresponding to negative shell energy are shaded, and the contour separation is 1 MeV.

DISCUSSION

For the first time we observed the linear structures meeting the condition $M_1 + M_2 = \text{const}$ in our experiment (Ex3) at the FOBOS setup based on the gas-filled detectors [9]. The linear ridges corresponding to the constant missing masses were revealed as a fine structure in the mass correlation plot collected with good statistics. Later using the COMETA spectrometer based on the mosaics of PIN diodes, we also observed the structures under discussion (Ex2), but the data suffered from small statistics [1]. Parameters of all linear structures observed so far in the region of so called "Ni-bump" are presented in Table 1. As can be inferred from Figure 5, showing the shell corrections map [10], the numbers of neutrons in the heavy magic cores (the forth column in Table 1) manifest themselves through the discussed structures correspond to the valley of negative shell corrections. In the recent publication [11] on the study of pear-shaped nuclei, it was noted that octupole correlations enhanced at the magic neutron numbers 34, 56, 88, 134. Thus, it is reasonable to expect that the nuclei having 116–134 neutrons would be pear-shaped and show magic properties. According to the calculations,

for instance [12], fissioning system becomes pear-shaped at the beginning of the descent from the fission barrier, at least in the most populated fission valley of the potential energy surface.

We propose the following scenario of the process leading to the formation of the structures under discussion. At the initial stage of the descent from the fission barrier the fissioning nucleus undergoes transformation from a prolate to more complicated shape. The nucleus of such shape consists of a heavy magic octupole deformed core and the light cluster in contact with the thin edge of the "pear". At further elongation the core takes dumb bell-like shape with more and more long neck between the heavy and light parts of the dumb bell. The mass of the light cluster stays unchanged. After the first rupture in the neck, a heavy fragment and a di-nuclear system consisting of the light cluster and some part of the neck fly apart. Later, due to the second rupture, the light cluster and the light FF become free. In general, the cinematics of the process seems to be similar to that discussed in [3].

CONCLUSIONS

Based on the new data we clarify a mechanism of the CCT mode similar to heavy ion radioactivity [9]: octupole deformed magic core plays the same role as magic Pb cluster in the "Lead radioactivity".

ACKNOWLEDGMENTS

This work was supported, in part, by the Russian Science Foundation and fulfilled in the framework of MEPhI Academic Excellence Project (Contract No. 02.a03.21.0005, 27.08.2013) by the Department of Science and Technology of the Republic of South Africa (RSA).

REFERENCES

1. Yu.V. Pyatkov et al., Eur. Phys. J. A 48 (2012) 94–110.
2. D.V. Kamanin, Yu. V. Pyatkov, "Clusters in Nuclei – Vol.3" ed. by C. Beck, Lecture Notes in Physics 875, pp. 183–246 (2013).
3. Yu.V. Pyatkov et al., Phys. Rev. C 96, №6, 064606 (2017).
4. Yu.V. Pyatkov et al., Proc. of the 25th Int. Seminar on Interaction of Neutrons with Nuclei, Dubna, Russia, 22-26 May 2017. Dubna 2018, p. 409-414.
5. D.V. Kamanin et al., Izvestiya Rossiiskoi Akademii Nauk. Seriya Fizicheskaya, 2018, V. 82, No. 6, pp. 804-807.
6. H.O. Neidel et al., Nucl. Instr. Meth. V. 178 (1980) P. 137.
7. S.I. Mulgin et al., NIM A 388 (1997) 254-259.
8. Yu.V. Pyatkov et al., Journal of Physics: Conference Series, V. 675, (2016), Int. Conf. on Particle Physics and Astrophysics (ICPPA-2015), 5–10 October 2015, Moscow, Russia, 042018.
9. Yu.V. Pyatkov et al., Eur. Phys. J. A 45 (2010) 29–37.
10. S. Aberg et al., Annu. Rev. Nucl. Part. Sci. 1990.40: 439-527.
11. L. P. Gaffne et al., Nature. V. 497 (2013).
12. Yu. V. Pyatkov, V. V. Pashkevich, et al., Nucl. Phys. A 624 (1997) 140.